3696 J. Med. Chem. 2010, 53, 3696–3706
DOI: 10.1021/jm100080z

Journal of Medicinal Chemistry Article

5,5′-Substituted Indirubin-3′-oxime Derivatives as Potent Cyclin-Dependent Kinase Inhibitors with Anticancer Activity

Soo-Jeong Choi,[†] Jung-Eun Lee,[†] Soon-Young Jeong,[‡] Isak Im,[†] So-Deok Lee,[†] Eun-Jin Lee,[§] Sang Kook Lee,[§,#] Seong-Min Kwon,[∥] Sang-Gun Ahn,[∥] Jung-Hoon Yoon,[∥] Sun-Young Han,[⊥] Jae-Il Kim,[†,‡] and Yong-Chul Kim*[,†,‡]

[†]*Department of Life Science, Gwangju Institute of Science and Technology, Gwangju 500-712, Republic of Korea,* [‡]*Division of Drug Discovery, Anygen Co., Ltd., Gwangju 500-712, Republic of Korea,* [§]*College of Pharmacy, Ewha Womans University, Seoul 120-759, Republic of Korea,* [∥]*Department of Pathology, School of Dentistry, Chosun University, Gwangju 501-759, Republic of Korea, and* [⊥]*Pharmacology Research Center, Korea Research Institute of Chemical Technology, Daejon 305-600, Republic of Korea.* [#]*Present address: College of Pharmacy, Seoul National University, Seoul, Republic of Korea*

Received January 19, 2010

To enhance the ability of indirubin derivatives to inhibit CDK2/cyclin E, a target of anticancer agents, we designed and synthesized a new series of indirubin-3′-oxime derivatives with combined substitutions at the 5 and 5′ positions. A molecular docking study predicted the binding of derivatives with OH or halogen substitutions at the 5′ position to the ATP binding site of CDK2, revealing the critical interactions that may explain the improved CDK2 inhibitory activity of these derivatives. Among the synthesized derivatives, the 5-nitro-5′-hydroxy analogue **3a** and the 5-nitro-5′-fluoro analogue **5a** displayed potent inhibitory activity against CDK2, with IC_{50} values of 1.9 and 1.7 nM, respectively. These derivatives also showed antiproliferative activity against several human cancer cell lines, with IC_{50} values of 0.2−3.3 μM. A representative analogue, **3a**, showed greater than 500-fold selectivity for CDK relative to selected kinase panel and potent in vivo anticancer activity.

Introduction

Cyclin-dependent kinases (CDKs) belong to a group of serine/threonine kinases involved in the regulation of cell cycle progression, neuronal function, differentiation, and apoptosis.[1] Their activity is tightly regulated by multiple mechanisms including binding to corresponding cyclins, of which level of expression oscillates throughout the different phases of the cell cycle.[2] Thus, different CDK/cyclin complexes are activated during each cell cycle step through G1, S, G2, and M phases. Sequential phosphorylation of the retinoblastoma protein (pRb) by CDK4/cyclin D and CDK6/cyclin D in early G1 phase and by CDK2/cyclin E in late G1 phase causes the release of the E2F proteins. These transcription factors, in turn, activate a set of genes required for entry into the S-phase of the cell cycle.[3,4] CDK2 is subsequently activated by cyclin A during the late stages of DNA replication in S-phase, and CDK2 promotes appropriately timed deactivation of E2F to prevent apoptosis triggered by persistent E2F activity.[5,6] Finally, CDK1, in a complex with cyclin A or B, is thought to be involved in regulating the G2/M checkpoint and driving cells through mitosis.[2,7]

In addition to playing roles in cell cycle control, CDK2, 7, 8, and 9 have been found to have other activities. For example, CDK2/cyclin E is important in the p53-mediated DNA damage response pathway, and CDK7, 8, and 9 are involved in the regulation of transcription initiation and elongation via phosphorylation of RNA polymerase.[8,9] Therefore, CDKs affect cell growth and survival through several mechanisms, making the appropriate regulation of CDK activity important in various cellular processes.

Deregulation of CDKs by abnormally high expression of cyclins, such as cyclins D and E, or by mutation, has been observed in many human tumors.[10] For example, the expression and catalytic activity of CDK2/cyclin E complexes is increased in colorectal, ovarian, breast, and prostate cancers, and elevated expression of cyclin E in primary tumors has been shown to correlate with poor survival rates in breast cancer patients.[11,12] Abnormal expression of CDK1/cyclin B complexes has also been observed in some patients with prostate adenocarcinoma and lung cancer.[13,14]

Although a report has shown that CDK2 may not be required for cell cycle progression and proliferation, recent reports suggested that melanocytes and hepatocytes may be dependent on CDK2 for proliferation and survival.[15−17] Also, an investigation of simultaneous depletion of CDK1 and CDK2 was reported to provide increased efficacy in antiproliferation of tumor cell lines, compared with targeting either CDK1 or CDK2 alone.[18] Furthermore, emerging evidence indicates that certain tumor cells may require specific interphase CDKs for proliferation.[7,15] Thus, inhibition of CDKs may provide an effective strategy for controlling tumor growth, making CDKs attractive targets for anticancer therapy.

At present, several small-molecule CDK inhibitors are undergoing clinical trials. These inhibitors are flat, small heterocyclic molecules that act by competing with ATP at the kinase ATP-binding site. Among these, flavopiridol was the first CDK inhibitor to enter clinical evaluations.[19] *R*-Roscovitine

*To whom correspondence should be addressed. Phone: 82-62-970-2502. Fax: 82-62-970-2484. E-mail: yongchul@gist.ac.kr.

Abbreviations: ATP, adenosine 5′-triphosphate; CDK, cyclin dependent kinase; DMEM, Dulbecco's Modified Eagle Medium; EI, electron impact; ESI, electro spray ionization; FAB, fast atom bombardment; HPLC, high-pressure liquid chromatography; HRMS, high-resolution mass spectroscopy; MOPS, 3-(*N*-morpholino)propanesulfonic acid; pRb, retinoblastoma protein; RPMI, Roswell Park Memorial Institute medium; SAR, structure−activity relationship; SRB sulforhodamine B.

 Published on Web 04/05/2010

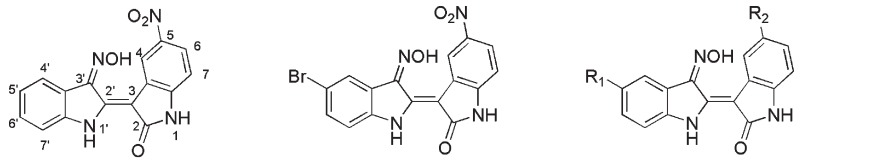

Figure 1. Structures of indirubin derivatives.

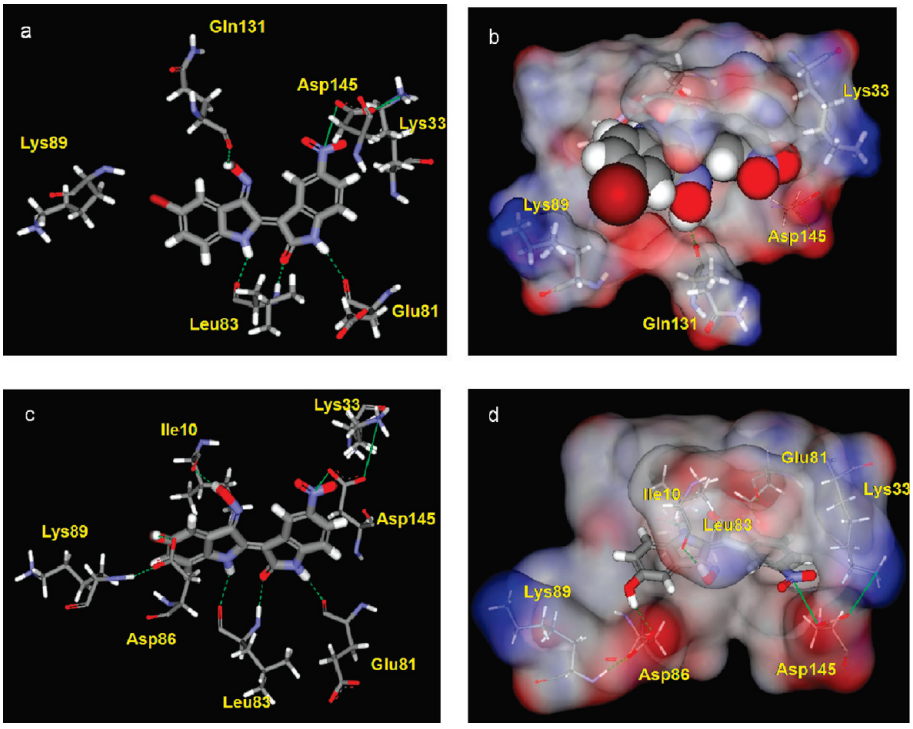

Figure 2. Binding mode of **2** and **3a** in the ATP binding site of CDK2. (a) Network of hydrogen bonds (green dashed lines) between **2** and the backbone amino acids in the ATP binding pocket of CDK2. Binding mode of **2** with CDK2 displays three hydrogen bonds between two nitrogen of **2** and Leu83 and Glu81 in the CDK2 hinge region, additional hydrogen bond between the oxime moiety and carbonyl oxygen of Gln131, and a salt bridge formed between 5-nitro group and the side chains of Lys33, Asp145. (b) van der Waals surface of CDK2 with **2** in CPK representation. 5′-Bromo group is projected toward the outer aqueous space of ATP binding pocket that presents a positively charged amino acid residue, Lys89. (c) Network of hydrogen bonds (green dashed lines) between **3a** and the backbone amino acids in the ATP binding pocket of CDK2. **3a** forms an additional hydrogen bond between the 5′-hydroxy group and the carboxylic acid of Asp86. This may further improve CDK2 inhibitory activity. (d) Molecular surface representation of CDK2 with **3a** bound in the ATP binding site. Some important amino acids lying within binding surface are displayed. The 5′-hydroxy group is pointing out of the pocket toward the solvent.

(a trisubstituted purine analogue)[20] and BMS-387032 (an aminothiazole)[21] are selective for CDK2/cyclin E, and PD-0332991 (a pyridopyrimidine)[22] is highly selective for CDK4/cyclin D and CDK6/cyclin D. Indirubin, a bis-indole scaffold and its derivatives, have been investigated with considerable interest as potent inhibitors targeting important protein kinases such as CDK, GSK-3β, and aurora kinases.[23−26] Our research group previously described the synthesis of a series of novel indirubin analogues and the evaluation of their antiproliferative and CDK2 inhibitory activities.[23] Recently, we also reported other activities of the indirubin derivatives including their regulation of cellular signaling through the inhibition of Notch-1 or activation of β-catenin-mediated Wnt signaling[27−29] and enhancing effect of differentiation of HL-60 leukemia cells induced by conventional activators such as 1,25-dihydroxyvitamin D3 and all-*trans* retinoic acid.[30]

Among the previously reported derivatives, 5-nitro-5′-bromo-indirubin-3′-oxime, **2**, showed the most potent antiproliferative activity (IC_{50} = 0.79−2.9 μM) against several cancer cell lines, with the additional substitution at the 5′ position enhancing activity when compared with the 5-nitro-indirubin-3′-oxime analogue, **1** (IC_{50} = 1.2−25.5 μM) (Figure 1). However, there are lack of reports regarding the synthesis and biological evaluations exploring the effect of various substitutions at the 5′ position of indirubin skeleton. We therefore performed a molecular docking study to design and synthesize novel 5,5′-substituted indirubin-3′-oxime analogues and assessed the biological properties of these molecules, including their CDK inhibitory, antiproliferative, and in vivo anticancer activities.

Results and Discussion

Molecular Docking for Designing Strategy. To address the mechanism behind the enhanced antiproliferative effect of compound **2**, we performed a molecular docking study on the ATP binding site of CDK2 (Figure 2) using CDOCKER, a CHARMm-based molecular dynamics docking program

Scheme 1. Synthesis of 5-Substituted Indoxyl-*N*,*O*-diacetate[a]

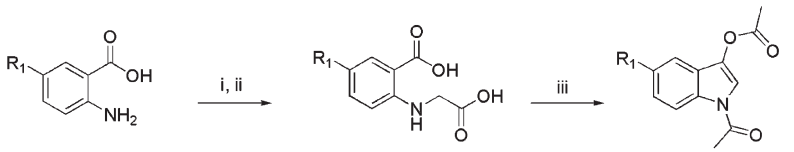

7a: R_1=OH
7b: R_1=Cl
7c: R_1=F
7d: R_1=CH_3

8a-d

9a: R_1=O-acetyl
9b: R_1=Cl
9c: R_1=F
9d: R_1=CH_3

[a] Reagents and conditions. (i) ethyl glyoxalate, $NaCNBH_3$, 1% acetic acid, methanol, room temp, 3 h, 85−95%; (ii) 1N NaOH (aq), methanol, room temp, 1 h, 90%; (iii) acetic anhydride, Na_2CO_3, reflux, 4 h, 65−72%.

Scheme 2. Synthesis of 5,5′-Substituted Indirubin-3′-oxime Derivatives[a]

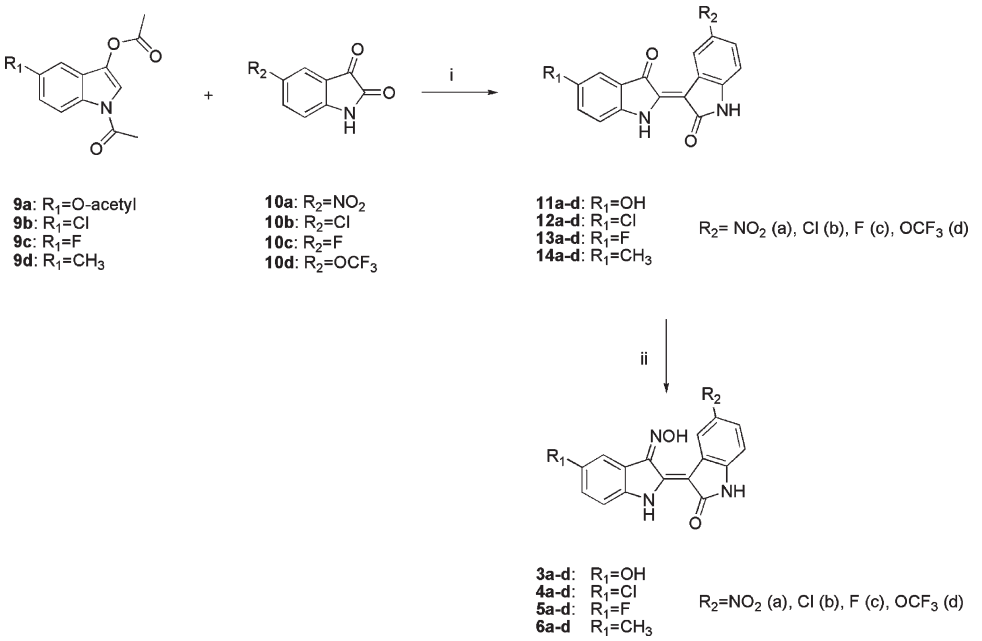

9a: R_1=O-acetyl
9b: R_1=Cl
9c: R_1=F
9d: R_1=CH_3

10a: R_2=NO_2
10b: R_2=Cl
10c: R_2=F
10d: R_2=OCF_3

11a-d: R_1=OH
12a-d: R_1=Cl
13a-d: R_1=F
14a-d: R_1=CH_3

R_2= NO_2 (a), Cl (b), F (c), OCF_3 (d)

3a-d: R_1=OH
4a-d: R_1=Cl
5a-d: R_1=F
6a-d R_1=CH_3

R_2=NO_2 (a), Cl (b), F (c), OCF_3 (d)

[a] Reagents and conditions. (i) Na_2CO_3, methanol or methanol: water (2:1), room temp, 2−3 h, 35−65%; (ii) $H_2NOH \cdot HCl$, pyridine, reflux, 0.5−3 h, 65−70%.

(Discovery Studio 2.0). The X-ray cocrystal structure of CDK2 with 5-bromoindirubin was obtained from the PDB data bank (PDB code: 2BHE).[31] After removing the ligand from the structure of complex, a binding sphere was constructed with a radius set as 8 Å. The final binding conformation of **2** was determined through molecular dynamics and final energy minimization. We found that the nitrogen at position 1′, the carbonyl oxygen at position 2, and the nitrogen at position 1 of compound **2** each formed a hydrogen bond with the hinge segments (Glu81, Leu83) of the ATP binding site (Figure 2a). In addition, the 3′-hydroxyl group of the oxime moiety formed a hydrogen bond with the backbone carbonyl of Gln131 and the 5-nitro group contributed to a salt bridge with the side chains of Lys33 and Asp145. A depiction of the binding surface with electrostatic potential within 4 Å around the ligand, **2**, showed that the 5′-Br group may be projected toward the outer aqueous space of the ATP binding pocket in which a positively charged amino acid residue, Lys89, may be a virtual binding partner (Figure 2b). It could be hypothesized that an additional electrostatic interaction between the lone pair electrons of the 5′-Br group and the positively charged Lys89 residue may result in a higher binding affinity with CDK2 and thus contribute to the more potent antiproliferative activity of **2** compared with the 5′-unsubstituted-indirubin-3′-oxime analogue, **1**. Results of the docking study show that derivatization at the 5′-position, along with 5-substituents (Cl, NO_2, F, and OCF_3) on the indirubin scaffold, may be an ideal strategy for optimizing binding affinity to CDK2.

To investigate the structure−activity relationships at the 5′ position of indirubin skeleton for CDK inhibitory and antiproliferative activities, following groups were selected for the derivatization: (1) 5′-F and 5′-Cl, which can form similar electrostatic interaction with Lys89 in a manner similar to that of the 5′-Br analogue, **2**, (2) 5′-OH, which can provide an additional hydrogen bond with CDK2 and introduce hydrophilic character at indirubin scaffold, (3) 5′-OCH_3 and 5′-CH_3, expecting contrast effects compared with halogen-substituted analogues.

A docking model of a representative molecule, 5-nitro-5′-hydroxy-indirubin-3′-oxime derivative (**3a**), in the ATP binding site of CDK2 (Figure 2c) showed that a new hydrogen bond may be formed between the 5′-OH group of **3a** and Asp86 in the solvent-accessible region of CDK2, with the oxime moiety of **3a** interacting with Ile10 instead of Gln131. A depiction of the binding surface with electrostatic

Scheme 3. Synthesis of 5-Substituted-5′-methoxy-indirubin-3′-oxime Derivatives[a]

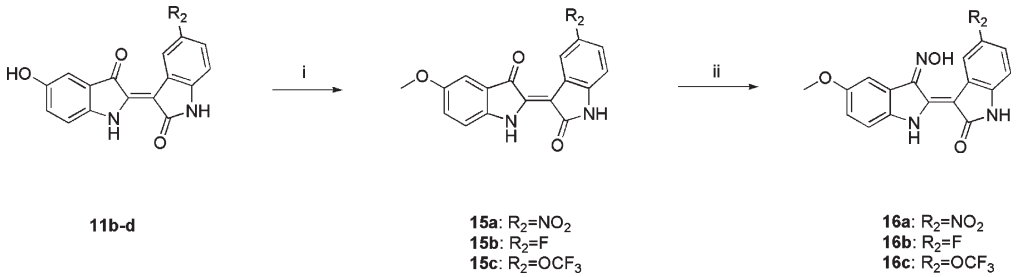

11b-d

15a: R_2=NO_2
15b: R_2=F
15c: R_2=OCF_3

16a: R_2=NO_2
16b: R_2=F
16c: R_2=OCF_3

[a] Reagents and conditions. (i) CH_3I, K_2CO_3, acetone, room temp, 4 h, 58−65%; (ii) $H_2NOH \cdot HCl$, pyridine, reflux, 0.5−3 h, 65−70%.

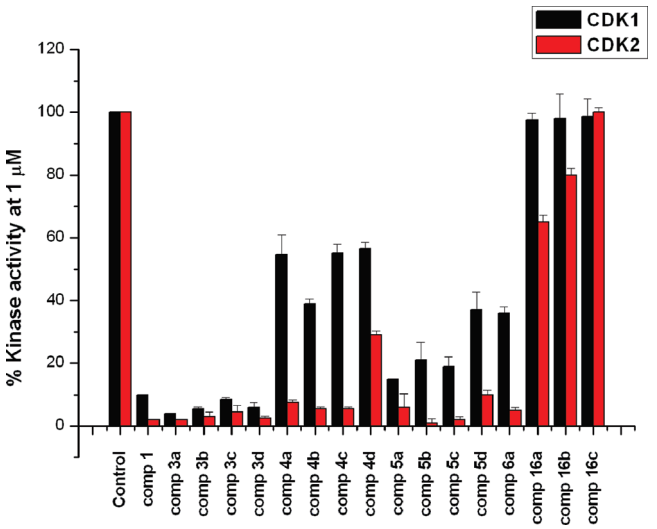

Figure 3. CDK1 and CDK2 % activity in the presence of 1 μM of 5,5′-substituted indirubin-3′-oxime derivatives. New indirubin derivatives (1 μM) were tested for their inhibitory effects in the kinase activity of CDK1/cyclin B and CDK2/cyclin E. 5-Nitroindirubin-3′-oxime (**1**) was also tested for comparison. Results are presented as the mean ± standard error of the mean (SEM) of the % kinase activity of CDK1 and CDK2.

potential within 4 Å around **3a** showed that the 5′-OH protrudes into the outer aqueous surface, solvent-accessible region (Figure 2d).

Chemistry. To synthesize the 5,5′-substituted-3′-indirubin oxime derivatives, the 5-substituted indoxyl-*N*,*O*-diacetates, **9a**−**d** were prepared from their corresponding 5-substituted anthranilic acids, **7a**−**d** with hydroxyl, chloro, fluoro, and methyl groups, respectively (Scheme 1). Briefly, each compound of **7a**−**d** was subjected to conditions of reductive alkylation with ethylglyoxalate, followed by hydrolysis to yield the dicarboxylic acids, **8a**−**d**. These latter compounds were finally cyclized in acetic anhydride[32] to yield acetoxy, chloro, fluoro, and methyl substituted compounds, **9a**−**d**. For the 5-hydroxy analogue, the cyclized compound **9a** was obtained as a triacetate form as the phenolic hydroxyl group was also acetylated under the cyclization conditions.

As described previously,[23] the 5,5′-substituted-3′-indirubin oxime derivatives **3**−**6** were synthesized from conjugate reactions of the 5-substituted indoxyl-*N*,*O*-diacetates **9a**−**d** with 5-nitro, chloro, fluoro, and trifluoromethoxy substituted isatin analogues **10a**−**d** under basic conditions to yield the 5,5′-substituted indirubin derivatives **11**−**14**, followed by the reaction of each of the latter with hydroxylamine to convert the ketone groups to 3′-oxime (Scheme 2). The 5-substituted-5′-methoxy-3′-oxime compounds **16a**−**c** were

Table 1. CDK2/Cyclin E iInhibitory Activities of 5,5′-Substituted Indirubin-3′-oxime Derivatives

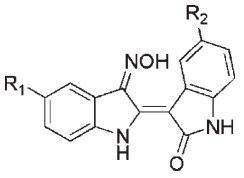

compd	R_1	R_2	IC_{50} (nM)[a]
3a	OH	NO_2	1.91 ± 0.16[b]
3b	OH	Cl	5.27 ± 0.51
3c	OH	F	2.25 ± 0.25
3d	OH	OCF_3	8.32 ± 0.27
4a	Cl	NO_2	23.5 ± 4.34[b]
4b	Cl	Cl	11.1 ± 0.89
4c	Cl	F	10.1 ± 0.86
4d	Cl	OCF_3	76.2 ± 2.31
5a	F	NO_2	1.71 ± 0.22
5b	F	Cl	8.01 ± 0.31
5c	F	F	1.83 ± 0.23
5d	F	OCF_3	60.3 ± 11.5
6a	CH_3	NO_2	8.68 ± 1.48
16a	OCH_3	NO_2	2,950 ± 530
16b	OCH_3	F	4,120 ± 450
16c	OCH_3	OCF_3	8,620 ± 870
1	H	NO_2	7.35 ± 0.21

[a] A series of indirubin derivatives were tested at 10 concentrations in CDK2/cyclin E kinase assay, as described in the Experimental Section. IC_{50} values were calculated from the dose−response curves. [b] IC_{50} values of **3a** and **4a** in CDK1/cyline B kinase assay are 13 nM and 195 nM, respectively .

synthesized from their corresponding 5-nitro, fluoro, and trifluoromethoxy substituted 5′-hydroxy-indirubin derivatives **15a**−**c** by methylation of the phenolic hydroxyl groups and subsequent reaction with hydroxylamine (Scheme 3).

CDK Inhibitory Activity and Kinase Selectivity Profile. The 5,5′-substituted-indirubin-3′-oxime derivatives were initially evaluated for their inhibitory activities against CDK1/cyclinB and CDK2/cyclinE at 1 μM (Figure 3). 5-Nitroindirubin-3′-oxime, **1**, was tested together for the comparison of the effects of substitutions at the 5′-position. The inhibitory activity and selectivity of the synthesized compounds for CDK2 over CDK1 were dependent on the nature of the 5′-substitutents at the R_1 position. In general, 5,5′-substituted indirubin-3′-oxime derivatives showed potent inhibitory activities against CDK2 with more than 90% inhibitory potency in 1 μM, except for **4d**, **16a**−**c**. Especially, 5′-OH analogues, **3a**−**d** showed the highest inhibitory activities against both CDK1 and CDK2. Although a substitution of hydroxyl group at the R_1 position resulted in decreased

selectivity for CDK2 over CDK1, simultaneous inhibition of CDK1 and CDK2 may have additional benefits in terms of anticancer activity according to the literature.[15,18,33] Moreover, the 5′-OH group improved the water solubility of compound **3a** about 30-fold compared with compounds **1** or **2** (the data of water solubility of compounds **1**, **2**, and **3a** was shown in Supporting Information, Table S3). Low-level water solubility has been a major problem among the physicochemical properties of indirubin analogues (data not shown). In contrast to the 5′-OH-substituted indirubin-3′-oxime derivatives, the 5′-chloro and 5′-fluoro-substituted derivatives **4a**−**d** and **5a**−**d** showed potent CDK2 inhibitory activities, with 6−10-fold selectivity compared to CDK1. For example, the 5-nitro-5′-chloro-indirubin-3′-oxime **4a** was about 8-fold more potent against CDK2 than CDK1 (Table 1). The decreased CDK1 inhibition resulting from 5′-halogenation is further supported by results showing that the 5-nitro-5′-bromo-indirubin-3′-oxime, **2**, had decreased CDK1 inhibitory activity (IC_{50} = 190 nM) when compared with the 5-nitro-indirubin-3′-oxime, **1**.[34] Among the series of compounds with electron-donating groups at the 5′ position, **6a**, with a 5′-CH_3 group, showed potent CDK2 inhibitory activity, with 7-fold selectivity over CDK1. However, at 1 μM, the 5′-OCH_3-substituted derivatives (**16a**−**c**) displayed weak or no inhibitory activities against CDK1 and CDK2.

The structure−activity relationships of 5,5′-indirubin-3′-oxime derivatives for their CDK2 inhibitory activities were analyzed with IC_{50} values (Table 1). We found that most derivatives, except for the 5′-OCH_3 compounds **16a**−**c**, showed potent inhibitory activities, with IC_{50} values of 1−70 nM. Regarding the effects of 5′-substituents at R_1

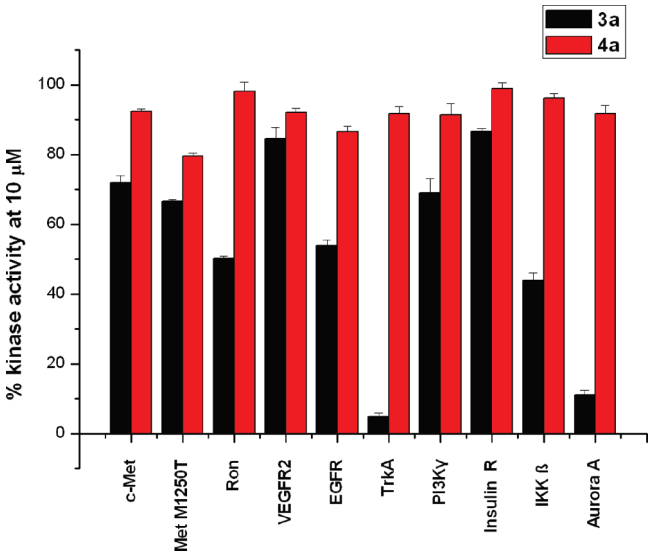

Figure 4. Kinase panel screening of **3a**, **4a**. Compounds **3a** and **4a** (10 μM) were tested against more diverse panel of kinases comprising of receptor tyrosine kinases, serine/threonine kinases, and lipid kinase. Results are presented as the mean ± standard error of the mean (SEM) of the % kinase activity. **3a** showed 9% inhibitory activity against TrkA at 1 μM. IC_{50} values of **3a** against two serine/threonine kinases, Aurora A (1 μM) and IKKβ (10 μM), and a receptor tyrosine kinase, TrkA (4 μM) were calculated from the dose−response curves.

Table 2. Antiproliferative Activities of 5,5′-Substituted Indirubin-3′-oxime Derivatives on Different Human Cancer Cell Lines[a]

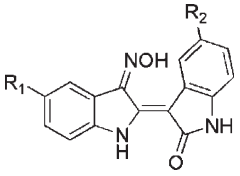

			IC_{50} (μM)						
compd	R_1	R_2	A549[b]	HT1080[c]	HCT116[d]	K562[e]	SNU638[f]	KB[g]	MCF-7[h]
3a	OH	NO_2	3.33	0.45	0.44	0.91	1.03	1.33	1.21
3b	OH	Cl	16.4	2.92	3.51	12.2	5.14	10.2	10.7
3c	OH	F	4.09	0.68	1.66	1.42	2.11	4.62	2.61
3d	OH	OCF_3	16.9	2.28	2.25	5.91	2.96	5.81	4.23
4a	Cl	NO_2	15.6	1.25	0.33	0.56	1.16	1.11	0.51
4b	Cl	Cl	> 20	12.2	1.86	17.2	2.57	11.9	6.14
4c	Cl	F	18.9	3.62	1.72	14.7	2.28	3.62	3.52
4d	Cl	OCF_3	> 20	17.7	3.79	> 20	2.71	2.83	4.23
5a	F	NO_2	0.57	0.64	0.28	0.46	0.94	0.92	0.91
5b	F	Cl	> 20	5.33	3.31	7.14	6.32	9.11	7.13
5c	F	F	10.3	8.62	13.5	15.9	2.23	13.2	6.57
5d	F	OCF_3	19.9	3.95	1.51	1.53	1.89	3.81	4.12
6a	CH_3	NO_2	> 20	3.92	1.41	0.81	1.06	2.11	1.06
6b	CH_3	Cl	> 20	> 20	18.8	> 20	12.7	5.18	8.79
6c	CH_3	F	> 20	> 20	> 20	> 20	11.5	10.6	10.5
6d	CH_3	OCF_3	> 20	> 20	> 20	> 20	> 20	8.13	7.31
16a	OCH_3	NO_2	> 20	> 20	> 20	> 20	> 20	> 20	> 20
16b	OCH_3	F	6.71	4.84	3.59	5.29	13.6	> 20	> 20
16c	OCH_3	OCF_3	> 20	> 20	> 20	> 20	> 20	20	13.2
2[i]	Br	NO_2	16.9	1.45	0.45	0.77	1.14	1.16	0.95
Roscovitine[i]			14.7	16.8	17.8	> 20	9.77	30.1	14.7

[a] A series of indirubin derivatives were tested at five concentrations for their effects on various human cancer cell lines using SRB assay, as described in the Experimental Section. The IC_{50} (μM) values were calculated from dose response curves and SD was described in the Supporting Information. [b] Human lung cancer cell. [c] Human fibro sarcoma cell. [d] Human colon cancer cell. [e] Human leukemia cell. [f] Human stomach cancer cell. [g] Human nasopharyngeal cancer cell. [h] Human breast cancer cell. [i] Experiments were also performed with **2** and Roscovitine as positive control.

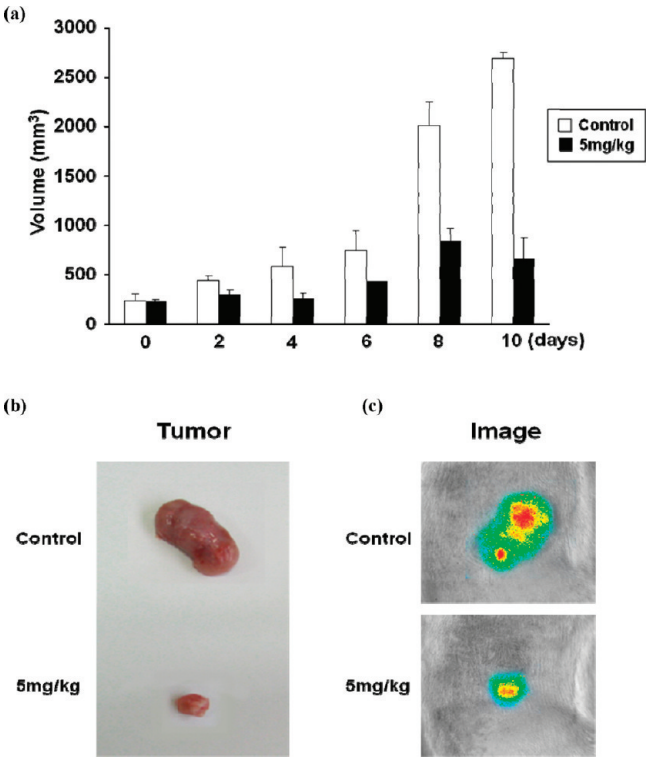

Figure 5. Inhibition of tumor growth by **3a**. (a) The SD-rats were injected with RK3E-ras-Luc cells ($5 \times 10^6/100\,\mu$L). When the tumor reached 5 mm in size, the rats were injected intravenously with **3a** (5 mg/kg) in nonanesthesia states every other day for a total of five times. The tumor size was measured by caliper as described in the Experimental Section. (b) Representative excised subcutaneous tumor from the control and **3a** treated rats. (c) In vivo bioluminescence imaging assay from the control and **3a** treated rats.

position, the CDK2 inhibitory activities increased in the following order: $-OCH_3 < -Cl < -H, -CH_3 < -OH, -F$. For example, the CDK2 inhibitory activities of the 5′-chloro-substituted-indirubin-3′-oxime compounds **4a**−**d** were 10-fold lower (IC_{50} = 10−76 nM) than were those of the 5′-fluoro-indirubin-3′-oxime derivatives **5a**−**c** (IC_{50} = 1−8 nM). Substitution of an electron-donating group, 5′-OCH_3 (**16a**−**c**), dramatically reduced CDK2 inhibitory activities with IC_{50} values of 2−8 μM, whereas substitution of another electron-donating group, 5′-CH_3 (**6a**), enhanced inhibitory activity 270-fold compared with **16b**. Particularly, the most potent CDK2 inhibitors, **3a**, **5a**, and **5c** had IC_{50} values against CDK2 of approximately 2 nM, thus demonstrating about a 4-fold greater potency than the 5-nitro-5′-unsubstituted-indirubin-3′-oxime, **1** (IC_{50} = 7 nM). Analysis of the effects of 5-substitution at the R_2 position of indirubin-3′-oxime derivatives showed that nitro or fluoro group generally enhanced CDK2 inhibition, compared with chloro or trifluoromethoxy group substitution. Together, our findings show that indirubin-3′-oxime analogues with combination of substituents providing electronic effects, such as OH or F at the 5′-position and NO_2 or F at the 5-position, displayed potent inhibitory activities against CDK2.

We further evaluated the representative potent and selective CDK2 inhibitors **3a** and **4a** against a diverse panel of receptor tyrosine kinases, serine/threonine kinases, and lipid kinase (Figure 4). Compound **3a** showed weak inhibitory activity only against Aurora A (IC_{50} = 1 μM), IKKβ (IC_{50} = 10 μM), and TrkA (IC_{50} = 4 μM), whereas compound **4a** displayed negligible inhibitory activities against all tested kinases. As the IC_{50} values of **3a** and **4a** against CDK1 and CDK2 were in the low nanomolar range, the kinase selectivity profiles of these compounds may be significantly favorable for CDK1 and CDK2.

Antiproliferative Activity. We tested the ability of the 5,5′-substituted indirubin-3′-oxime derivatives to inhibit the proliferation of several cancer cell lines, including A549, HT1080, HCT116, K562, SNU638, KB, and MCF-7, using SRB assay, and compared the data with the positive controls 5-nitro-5′-bromo-indirubin-3′-oxime (**2**) and Roscovitine (Table 2).

We found that the antiproliferative activities of the 5′-hydroxy derivatives **3a**−**d** were well correlated with their ability to inhibit CDK2, with activities depending on the substituents at the 5 position, in the order NO_2 > F > Cl, OCF_3. In particular, the 5-nitro-5′-hydroxy-indirubin-3′-oxime **3a** showed similar or greater inhibitory activity than did compound **2**, depending on the cell line tested, with IC_{50} values of ~0.4 μM against the HT1080 and HCT116 cell lines. Among compounds in which the 5′-bromo group of **2** was replaced by other halogen groups, such as Cl or F, the 5-nitro analogues **4a** and **5a** were especially effective against the HCT116 human colon cancer cell line in which cyclin D1 is deregulated,[35] with IC_{50} values of approximately 0.3 μM. The 5-nitro-5′-fluoro-indirubin-3′-oxime **5a** showed the broadest spectrum of inhibitory activity against all cancer cell lines, with IC_{50} values of 0.28−0.94 μM, and the values correlated with activity against CDK2. Compound **5a** was the only derivative to show a nanomolar IC_{50} value against the A549 human lung cancer cell line, in contrast to the weak antiproliferative activities of most other derivatives. Although the majority of the indirubin-3′-oxime derivatives substituted with electron-donating groups such as 5′-CH_3 or 5′-OCH_3 (**6** and **16**) were very weak inhibitors of cancer cell lines, the 5-nitro-5′-methyl-3′-oxime **6a** had antiproliferative IC_{50} values in the range of 0.8−1 μM. Regarding the substitutions at the 5-position (R_2), the 5-NO_2 group in combination with 5′-OH, Cl, F, or CH_3 showed the most potent antiproliferative activity among the 5,5′-disubsituted derivatives tested. These findings are in good agreement with our previous results[23] and are supported by the hypothesized binding mode of **2** and **3a**, in which an additional salt bridge may form between the 5-nitro group and Asp145 and Lys33 in the ATP binding site of CDK2. Among the 5′-OCH_3 derivatives, only the 5-F substituted analogue **16b** displayed moderate antiproliferative activity, indicating that this analogue may have a different mechanism of action. Our combined results suggest that 5′-hydroxyl or halogen groups may enhance the inhibition of CDK and cancer cell growth, possibly by forming additional hydrogen bond or electrostatic interaction at the ATP binding site of CDK2.

In Vivo Anticancer Activity of 3a. To assess the in vivo activity of the indirubin analogue, we utilized an animal tumor model in which Sprague−Dawley (SD) rats were subcutaneously transplanted with RK3E-ras rat kidney cells harboring the k-ras and GFP/Luc genes, as published by our group.[36] The 5-nitro-5′-hydroxy analogue, **3a**, was selected for in vivo test because the improved water solubility of **3a** while maintaining the potent CDK inhibitiory and antiproliferative activity compared with other derivatives, which usually precipitated in the bloodstream of animals when administered through tail vein. Five days after transplantation, 5 mg/kg **3a** was administered iv to each animal every

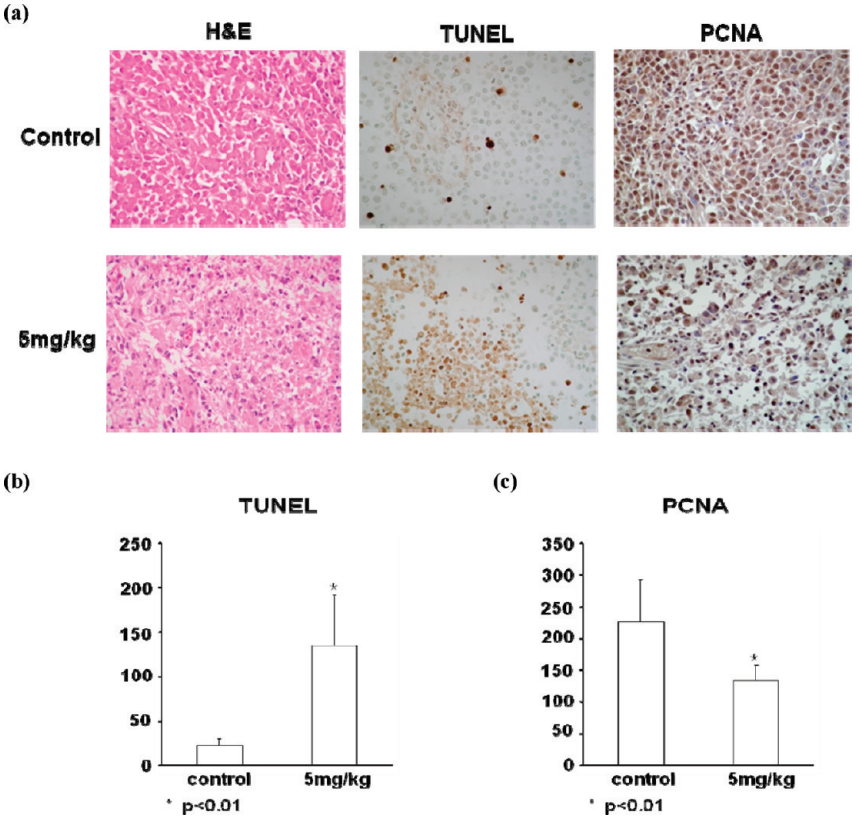

Figure 6. Histology and immunohistochemistry of tumor tissue. RK3E-ras-Luc cells were inoculated sc on the left flank of rats. **3a** (5 mg/kg) was injected intravenously into the tumor bearing rats every other day beginning from day 5. The rats were sacrificed on day 11. (a) H&E staining of tumor sections (left), TUNEL assay on paraffin sections from solid tumor (center), and immunohistochemical staining for PCNA (right), (b) positive cells for TUNEL assay, (c) positive cells for PCNA immunostaining. Cells were counted in triplicate. Columns, mean; bars, SD.

other day with a total of five times and the rats were monitored daily. We found that tumor volume was significantly decreased, by about 84.3%, compared with control rats (Figure 5a,b). There was no significant difference in body weight between **3a**-treated and control rats (data not shown). Bioluminescence images obtained on day 10 after treatment with **3a** indicated that luminescence intensity, an indicator of tumor growth, was significantly decreased (Figure 5c).

Histological analysis showed that untreated control solid tumors were anaplastic undifferentiated carcinomas, showing many mitotic figures, multifocal necrosis, and hemorrhage. Tumor treatment with **3a**, however, led to extensive cell death (Figure 6a, left) and a 6-fold increase in the number of TUNEL-positive apoptotic cells (Figure 6a, center, and Figure 6b). In contrast, the level of expression of PCNA, a cell proliferation marker, was lower in **3a**-treated animals than in controls (Figure 6a, right, and Figure 6c). In addition, a result of cell cycle analysis using FACS showed that **3a** inhibited cell cycle progression at the G_0/G_1 phase in RK3E-ras rat kidney cells (The data of cell cycle distribution is shown in Supporting Information, Figure S1).

These results indicate that **3a** suppresses tumor growth in vivo by inhibiting cell proliferation and activating apoptosis. Although the in vitro and in vivo anticancer activity of **3a** was correlated with the CDK inhibitory activity, a possibility of combined mechanisms of the action could be speculated from several reports of molecular mechanisms of indirubin derivatives in anticancer activity such as inhibition of Notch-1 or Stat3 signaling and promoting caspase activity via a mitochondria-mediated pathway.[27,28,37,38]

Conclusions

In summary, we describe here the design and synthesis of several novel 5,5′-substituted-indirubin-3′-oxime compounds as potent inhibitors of CDK1 and CDK2 and with antiproliferative activities against several cancer cell lines. The enhanced inhibitory activities of these 5,5′-substituted derivatives, compared with the 5′-unsubstituted indirubin-3′-oxime **1**, could be interpreted based on the results of a molecular docking study at the ATP binding site of CDK2, showing that the substituted derivates showed additional projections into the solvent-accessible region and additional interactions with the amino acid residues in the ATP binding pocket, as exemplified by the 5′-hydroxy analogue **3a**. The most potent CDK2 inhibitors were 5-nitro-5′-hydroxy-indirubin-3′-oxime (**3a**) and 5-nitro-5′-fluoro-indirubin-3′-oxime (**5a**), which had IC_{50} values of 1.91 and 1.71 nM, respectively, and IC_{50} values in the range of 0.2−3.3 μM when tested as antiproliferative agents against several human cancer cell lines. Structure−activity relationship analysis showed that OH and halogen groups were preferred to the electron donating groups such as 5′-CH_3, 5′-OCH_3 at 5′ position. A representative analogue, 5-nitro-5′-hydroxy-indirubin-3′-oxime (**3a**), showed greater than 500-fold selectivity for CDK relative to selected kinase panel, and significant in vivo anticancer activity. These findings may contribute to the design and development of CDK inhibitors and facilitate clinical application.

Experimental Section

Chemistry. ^{1}H NMR spectra were determined with a JEOL JNM-LA 300WB spectrometer at 300 MHz or JEOL

JNM-ECX 400P spectrometer at 400 MHz, and spectra were taken in $CDCl_3$ or DMSO-d_6 or acetone-d_6. Unless otherwise noted, chemical shifts are expressed as ppm downfield from internal tetramethylsilane, or relative ppm from DMSO (2.5 ppm), acetone (2.04 ppm). Mass spectroscopy was carried out on electrospray and high-resolution mass spectra (m/z) were recorded on a FAB, EI (JEOL: mass range 2600 amu, 10 kV acceleration) and ESI. High-resolution mass analysis was performed at Korea Basic Science Institute (Daegu).

The purity of all final products was determined by HPLC (at least 95% purity unless otherwise noted). The determination of purity was performed on a Shimadzu SCL-10A VP HPLC system using a Shimadzu Shim-pack C18 analytical column (250 mm × 4.6 mm, 5 mm, 100 Å) in linear gradient solvent systems. Solvent system was H_2O:CH_3CN = 65:35 to 5:95 over 30 min at a flow rate = 1 mL/min. Peaks were detected by UV absorption using a diode array detector.

General Procedure for the Preparation of 5-Substituted indoxyl-*N*,*O*-diacetate 9a−d. To a solution of 5-substituted anthranilic acid (1.0 g, 6.45 mmol) in 50 mL of methanol was added 0.5 mL of acetic acid, followed by ethyl glyoxalate (1 mL, 9.7 mmol) and $NaCNBH_3$ (609.5 mg, 9.7 mmol). The reaction mixture was stirred for 3 h at room temperature. Then the methanol was removed by evaporation. The residue was taken up in solution of saturated NH_4Cl in water and extracted with ethyl acetate. The combined extracts were dried over sodium sulfate, filtered, and evaporated. The residue was purified by silica gel column chromatography (CH_3Cl:methanol = 30:1) to give ester product (1.4 g, 95%) and then this compound (1.4 g, 5.8 mmol) was hydrolyzed in 25 mL of 1 N NaOH(aq) and 10 mL of methanol. The reaction mixture was stirred for 1 h at room temperature, and the resulting solution was acidified by 1N HCl. The resulting precipitate (1.2 g, 90%) was collected by filtration and washed with water. To the obtained diacid compounds **8a−d** (1.2 g, 4.97 mmol) was added acetic anhydride (15 mL) and Na_2CO_3 (1.3 g, 12.4 mmol). The reaction mixture was refluxed for 4 h, and the product was extracted with ethyl acetate and washed with water. The combined extracts were dried over sodium sulfate, filtered, and evaporated. The residue was purified by silica gel column chromatography (hexane:ethyl acetate =2:1) to give **9a−d** with 5-acetoxy, chloro, fluoro, and methyl groups, respectively (800 mg, 68%).

Data for 1-Acetyl-1*H*-indole-3, 5-diyl Diacetate (9a). ^{1}H NMR ($CDCl_3$, 300 MHz, δ ppm, J in Hz) 8.46 (1H, d, J = 9.3 Hz), 7.76 (1H, s), 7.30 (1H, d, J = 2.4 Hz), 7.11 (1H, dd, J = 9.3, 2.4 Hz), 2.67 (3H, s), 2.36 (3H, s), 2.31 (3H, s). ESI $[M - H]^-$: 273.83.

Data for 1-Acetyl-5-chloro-1*H*-indol-3-yl Acetate (9b). ^{1}H NMR ($CDCl_3$, 400 MHz, δ ppm, J in Hz) 8.40 (1H, d, J = 8.8 Hz), 7.75 (1H, s), 7.53 (1H, d, J = 2 Hz), 7.34 (1H, dd, J = 8.8, 2 Hz), 2.61 (3H, s), 2.39 (3H, s). ESI $[M - H]^-$: 249.83.

Data for 1-Acetyl-5-fluoro-1*H*-indol-3-yl Acetate (9c). ^{1}H NMR ($CDCl_3$, 400 MHz, δ ppm, J in Hz) 8.42 (1H, m), 7.75 (1H, s), 7.19 (1H, dd, J = 8.2, 2.4 Hz), 7.10 (1H, td, J = 8.8, 2.4 Hz), 2.59 (3H, s), 2.37 (3H, s). ESI $[M - H]^-$: 233.88.

Data for 1-Acetyl-5-methyl-1*H*-indol-3-yl Acetate (9d). ^{1}H NMR ($CDCl_3$, 400 MHz, δ ppm, J in Hz) 8.31 (1H, d, J = 7.6 Hz), 7.65 (1H, s), 7.31 (1H, s), 7.19 (1H, d, J = 7.6 Hz), 2.57 (3H, s), 2.44 (3H, s), 2.36 (3H, s). ESI $[M - H]^-$: 229.80.

General Procedure for the Preparation of 5,5′-Substituted Indirubin-3′-oxime Derivatives 3−6. To a solution of 5-nitro, chloro, fluoro, and trifluoromethoxy substituted isatin analogues **10a−d** (77 mg, 0.425 mmol) in methanol (5 mL) were added 5-substituted indoxyl-*N*,*O*-diacetate **9a−d** (100 mg, 0.425 mmol) and the mixture was stirred for 5 min. Anhydrous Na_2CO_3 (112.5 mg, 1.06 mmol) was added, and the stirring was continued for 3 h at room temperature. The dark precipitate was filtered and washed with cold water and dried under reduced pressure to give derivatives of 5,5′-substituted indirubin (63 mg, 47%), **11−14**. The indirubin derivative (10 mg, 0.032 mmol) was dissolved in pyridine (0.3 mL), and hydroxylamine hydrochloride (6.6 mg, 0.095 mmol) was added. The reaction mixture was heated under reflux at 120 °C for 2 h. After cooling, the solution was acidified with 1N HCl and the resulting precipitate was filtered and washed with water to afford quantitatively the corresponding 3′-oxime selectively in a (2′*Z*,3′*E*) form. The residue was purified by silica gel column chromatography (chloroform:methanol = 20:1) to give **3−6** (7 mg, 66%).

Data for (2′*Z*,3′*E*)-5-Nitro-5′-hydroxy-indirubin-3′-oxime (3a). ^{1}H NMR (DMSO, 300 MHz, δ ppm, J in Hz) 13.87 (1H, s, NOH), 11.78 (1H, s, N-H), 11.35 (1H, s, N′-H), 9.41 (1H, d, J = 2.8 Hz, H-4), 9.32 (1H, s, O-H), 8.05 (1H, dd, J = 11.6, 2.8 Hz, H-6), 7.76 (1H, d, J = 3.2 Hz, H-4′), 7.29 (1H, d, J = 11.6 Hz, H-7), 7.04 (1H, d, J = 11.2 Hz, H-7′), 6.86 (1H, dd, J = 11.2, 3.2 Hz, H-6′). HRMS (EI) $[M]^{+\bullet}$ ($C_{16}H_{10}N_4O_5$): calcd 338.0651, found 338.0648.

Data for (2′*Z*,3′*E*)-5-Chloro-5′-hydroxy-indirubin-3′-oxime (3b). ^{1}H NMR (DMSO, 400 MHz, δ ppm, J in Hz) 11.71 (1H, s, N-H), 10.78 (1H, s, N′-H), 9.27 (1H, s, O-H), 8.59 (1H, d, J = 2 Hz, H-4), 7.74 (1H, d, J = 2 Hz, H-4′), 7.24 (1H, d, J = 8.4 Hz, H-7), 7.11 (1H, dd, J = 8, 2 Hz, H-6′), 6.87 (1H, d, J = 8.4 Hz, H-6), 6.85 (1H, d, J = 8 Hz, H-7′). HRMS (EI) $[M]^{+\bullet}$ ($C_{16}H_{10}ClN_3O_3$): calcd 327.0411, found 327.0408. Purity 92%.

Data for (2′*Z*,3′*E*)-5-Fluoro-5′-hydroxy-indirubin-3′-oxime (3c). ^{1}H NMR (DMSO, 400 MHz, δ ppm, J in Hz) 11.69 (1H, s, N-H), 10.66 (1H, s, N′-H), 9.25 (1H, s, O-H), 8.42 (1H, dd, J = 11.4, 2.8 Hz, H-6), 7.73 (1H, d, J = 2.4 Hz, H-4′), 7.24 (1H, d, J = 8.4 Hz, H-6′), 6.81−6.99 (3H, m, H-7′, H-4, H-7). HRMS (EI) $[M]^{+\bullet}$ ($C_{16}H_{10}FN_3O_3$): calcd 311.0706, found 311.0707. Purity 93%.

Data for (2′*Z*,3′*E*)-5-Trifluoromethoxy-5′-hydroxy-indirubin-3′-oxime (3d). ^{1}H NMR (DMSO, 400 MHz, δ ppm, J in Hz) 11.70 (1H, s, N-H), 10.78 (1H, s, N′-H), 9.22 (1H, s, O-H), 8.50 (1H, s, H-4), 7.70 (1H, d, J = 2 Hz, H-4′), 7.21 (1H, d, J = 8.8 Hz, H-7′), 7.03 (1H, d, J = 8.4 Hz, H-7), 6.88 (1H, d, J = 8.4 Hz, H-6), 6.80 (1H, dd, J = 8.8, 2.4 Hz, H-6′). HRMS (ESI) $[M - H]^-$ ($C_{17}H_9F_3N_3O_4$): calcd 376.0545, found 376.0546.

Data for (2′*Z*,3′*E*)-5-Nitro-5′-chloro-indirubin-3′-oxime (4a). ^{1}H NMR (DMSO, 400 MHz, δ ppm, J in Hz) 11.98 (1H, s, N-H), 11.39 (1H, s, N′-H), 9.45 (1H, s, H-4), 8.25 (1H, s, H-4′), 8.08 (1H, d, J = 7.6 Hz, H-6), 7.50 (2H, m, H-6′, H-7), 7.05 (1H, d, J = 8.4 Hz, H-7′). HRMS (ESI) $[M - H]^-$ ($C_{16}H_8ClN_4O_4$): calcd 355.0234, found 355.0242.

Data for (2′*Z*,3′*E*)-5-Chloro-5′-chloro-indirubin-3′-oxime (4b). ^{1}H NMR (acetone, 300 MHz, δ ppm, J in Hz) 13.05 (1H, s, NOH), 11.82 (1H, s, N-H), 9.81 (1H, s, N′-H), 8.67 (1H, s, H-4), 8.35 (1H, d, J = 1.8 Hz, H-4′), 7.45 (2H, m, H-6, H-7), 7.16 (1H, d, J = 8.4 Hz, H-6′), 6.97 (1H, d, J = 8.4 Hz, H-7′). HRMS (EI) $[M]^{+\bullet}$ ($C_{16}H_9Cl_2N_3O_2$): calcd 345.0072, found 345.0075.

Data for (2′*Z*,3′*E*)-5-Fluoro-5′-chloro-indirubin-3′-oxime (4c). ^{1}H NMR (acetone, 300 MHz, δ ppm, J in Hz) 12.96 (1H, s, NOH), 11.78 (1H, s, N-H), 9.71 (1H, s, N′-H), 8.41 (1H, d, J = 11.4 Hz, H-7), 8.32 (1H, s, H-4), 7.40−7.50 (2H, m, H-4′, H-6′), 6.88−6.91 (2H, m, H-6, H-7′). HRMS (ESI) $[M - H]^-$ ($C_{16}H_8ClFN_3O_2$): calcd 328.0289, found 328.0291.

Data for (2′*Z*,3′*E*)-5-Trifluoromethoxy-5′-chloro-indirubin-3′-oxime (4d). ^{1}H NMR (acetone, 300 MHz, δ ppm, J in Hz) 13.02 (1H, s, NOH), 11.82 (1H, s, N-H), 9.88 (1H, s, N′-H), 8.63 (1H, s, H-4), 8.34 (1H, d, J = 2.1 Hz, H-4′), 7.47 (2H, m, H-6, H-7), 7.11 (1H, d, J = 8.4 Hz, H-6′), 7.03 (1H, d, J = 8.4 Hz, H-7′). HRMS (ESI) $[M - H]^-$ ($C_{17}H_8ClF_3N_3O_3$): calcd 394.0206, found 394.0215.

Data for (2′*Z*,3′*E*)-5-Nitro-5′-fluoro-indirubin-3′-oxime (5a). ^{1}H NMR (DMSO, 400 MHz, δ ppm, J in Hz) 11.89 (1H, s, N-H), 11.40 (1H, s, N′-H), 9.43 (1H, d, J = 2 Hz, H-4), 8.08 (1H, dd, J = 8.6, 2 Hz, H-6), 8.00 (1H, dd, J = 8.6, 2 Hz, H-7), 7.51 (1H, m, H-4′), 7.33 (1H, td, J = 9, 2.8 Hz, H-6′), 7.06 (1H, d, J = 8.4 Hz, H-7′). HRMS (EI) $[M]^{+\bullet}$ ($C_{16}H_9FN_4O_4$): calcd 340.0608, found 340.0610.

Data for (2′*Z*,3′*E*)-5-Chloro-5′-fluoro-indirubin-3′-oxime (5b). ^{1}H NMR (DMSO, 400 MHz, δ ppm, J in Hz) 11.81 (1H, s,

N-H), 10.85 (1H, s, N′-H), 8.62 (1H, d, J = 2.4 Hz, H-4), 7.97 (1H, dd, J = 8.2, 2.4 Hz, H-6), 7.47 (1H, m, H-4′), 7.31 (1H, m, H-7), 7.15 (1H, dd, J = 8.4, 2 Hz, H-6′), 6.88 (1H, d, J = 8.4 Hz, H-7′). HRMS (ESI) $[M - H]^-$ ($C_{16}H_8ClFN_3O_2$): calcd 328.0289, found 328.0295.

Data for (2′*Z*,3′*E*)-5-Fluoro-5′-fluoro-indirubin-3′-oxime (5c). ^{1}H NMR (DMSO, 400 MHz, δ ppm, J in Hz) 11.76 (1H, s, N-H), 10.68 (1H, s, N′-H), 8.41 (1H, dd, J = 11.2, 2.4 Hz, H-4), 7.93 (1H, dd, J = 8.8, 2.4 Hz, H-4′), 7.39 (1H, m, H-7), 7.30 (1H, td, J = 8.8, 2 Hz, H-6), 6.93 (1H, td, J = 9, 2.4 Hz, H-6′), 6.84 (1H, m, H-7′). HRMS (EI) $[M]^{+\bullet}$ ($C_{16}H_9F_2N_3O_2$): calcd 313.0663, found 313.0666. Purity 93%.

Data for (2′*Z*,3′*E*)-5-Trifluoromethoxy-5′-fluoro-indirubin-3′-oxime (5d). ^{1}H NMR (DMSO, 400 MHz, δ ppm, J in Hz) 12.02 (1H, s, N-H), 10.72 (1H, s, N′-H), 8.59 (1H, s, H-4), 8.02 (1H, dd, J = 8.8, 2.4 Hz, H-6), 7.41 (1H, m, H-4′), 7.18 (1H, td, J = 9.2, 2 Hz, H-6), 7.00 (1H, d, J = 8.4 Hz, H-7), 6.9 (1H, d, J = 8.4 Hz, H-7′). HRMS (FAB) ($C_{17}H_9O_3N_3F_4$): calcd 379.0579, found 379.0580.

Data for (2′*Z*,3′*E*)-5-Nitro-5′-methyl-indirubin-3′-oxime (6a). ^{1}H NMR (DMSO, 400 MHz, δ ppm, J in Hz) 11.87 (1H, s, N-−H), 11.38 (1H, s, N′-H), 9.46 (1H, d, J = 2.4 Hz, H-4), 8.11 (1H,s, H-4′), 8.07 (1H, dd, J = 8, 2.4 Hz, H-6), 7.37 (1H, d, J = 8 Hz, H-7), 7.26 (1H, d, J = 8.8 Hz, H-6′), 7.05 (1H, d, J = 8.8 Hz, H-7′), 2.32 (3H, s, CH_3). HRMS (ESI) $[M - H]^-$ ($C_{17}H_{11}N_4O_4$): calcd 335.0780, found 335.0787. Purity 93%.

Data for (2′*Z*,3′*E*)-5-Chloro-5′-methyl-indirubin-3′-oxime (6b). ^{1}H NMR (DMSO, 400 MHz, δ ppm, J in Hz) 11.85 (1H, s, N-H), 10.76 (1H, s, N′-H), 8.64 (1H, s, H-4), 8.10 (1H,s, H-4′), 7.29 (1H, d, J = 8.4 Hz, H-6), 7.20 (1H, d, J = 8.4 Hz, H-7), 7.10 (1H, d, J = 8.2 Hz, H-6′), 6.86 (1H, d, J = 8.4 Hz, H-7′), 2.31 (3H, s, CH_3). HRMS (EI) $[M]^{+\bullet}$ ($C_{17}H_{12}ClN_3O_2$): calcd 325.0618, found 325.0623.

Data for (2′*Z*,3′*E*)-5-Fluoro-5′-methyl-indirubin-3′-oxime (6c). ^{1}H NMR (DMSO, 400 MHz, δ ppm, J in Hz) 11.78 (1H, s, N-H), 10.61 (1H, s, N′-H), 8.43 (1H, dd, J = 11.2, 2.4 Hz, H-4), 8.06 (1H,s, H-4′), 7.26 (1H, d, J = 8.4 Hz, H-7), 7.17 (1H, d, J = 8 Hz, H-7′), 6.86 (1H, td, J = 8.4, 2.4 Hz, H-6), 6.80 (1H, d, J = 8 Hz, H-6′), 2.28 (3H, s, CH_3). HRMS (EI) $[M]^{+\bullet}$ ($C_{17}H_{12}FN_3O_2$): calcd 309.0914, found 309.0912.

Data for (2′*Z*,3′*E*)-5-Trifluoromethoxy-5′-methyl-indirubin-3′-oxime (6d). ^{1}H NMR (DMSO, 400 MHz, δ ppm, J in Hz) 11.80 (1H, s, N-H), 10.87 (1H, s, N′-H), 8.59 (1H, d, J = 2 Hz, H-4), 8.09 (1H,s, H-4′), 7.34 (1H, d, J = 8.4 Hz, H-6), 7.25 (1H, d, J = 8 Hz, H-7), 7.10 (1H, d, J = 7.4 Hz, H-6′), 6.94 (1H, d, J = 8.4 Hz, H-7′), 2.33 (3H, s, CH_3). HRMS (EI) $[M]^{+\bullet}$ ($C_{18}H_{12}F_3N_3O_3$): calcd 375.0831, found 375.0833.

General Procedure for the Preparation of 5-Substituted-5′-methoxy-indirubin-3′-oxime Derivatives 16a−c. To a solution of 5′-hydroxy-indirubin analogues, **11d** (10 mg, 0.028 mmol) in acetone (1 mL) were added dropwise methyl iodide (17 μL, 0.276 mmol) and K_2CO_3 (19 mg, 0.138 mmol). The mixture was stirred for 4 h at room temperature. The dark precipitate was filtered and washed with cold water and dried under reduced pressure to give derivatives of 5-substituted-5′-methoxy-indirubin (6 mg, 60%), **15c**. The indirubin derivative (6 mg, 0.016 mmol) was dissolved in pyridine (0.3 mL), and hydroxylamine hydrochloride (3.4 mg, 0.048 mmol) was added. The reaction mixture was heated under reflux at 120 °C for 1 h. After cooling, the product was acidified with 1N HCl and the precipitate was filtered and washed with water to afford quantitatively the corresponding 3′-oxime selectively in a (2′*Z*,3′*E*) form. The residue was purified by silica gel column chromatography (hexane:ethyl acetate = 2:1) to give **16a−c** (4 mg, 65%).

Data for (2′*Z*,3′*E*)-5-Nitro-5′-methoxy-indirubin-3′-oxime (16a). ^{1}H NMR (DMSO, 400 MHz, δ ppm, J in Hz) 11.82(1H, s, N-H), 9.46 (1H, d, J = 2.4 Hz, H-4), 9.33 (1H, s, N′-H), 8.12 (1H, dd, J = 8.4, 2.4 Hz, H-6), 7.77 (1H, d, J = 2.4 Hz, H-4′), 7.30 (1H, d, J = 8.4 Hz, H-7), 7.24 (1H, d, J = 9.2 Hz, H-7′), 6.85 (1H, dd, J = 7.8, 2.4 Hz, H-6′), 3.39 (3H, s, OCH_3). HRMS (ESI) $[M - H]^-$ ($C_{17}H_{11}N_4O_5$): calcd 351.0729, found 351.0724. Purity 94%.

Data for (2′*Z*,3′*E*)-5-Fluoro-5′-methoxy-indirubin-3′-oxime (16b). ^{1}H NMR (DMSO, 400 MHz, δ ppm, J in Hz) 11.68 (1H, s, N-H), 9.22 (1H, s, N′-H), 8.44 (1H, m, H-4), 7.70 (1H, d, J = 2.4 Hz, H-4′), 7.21 (1H, d, J = 8.8 Hz, H-6), 6.96 (2H, m, H-7, H-7′), 6.79 (1H, dd, J = 8.6, 2.4 Hz, H-6′), 3.26 (3H, s, OCH_3). HRMS (EI) $[M]^{+\bullet}$ ($C_{17}H_{12}FN_3O_3$): calcd 325.0863, found 325.0859.

Data for (2′*Z*,3′*E*)-5-Trifluoromethoxy-5′-methoxy-indirubin-3′-oxime (16c). ^{1}H NMR (acetone, 400 MHz, δ ppm, J in Hz) 11.70 (1H, s, N-H), 8.62 (1H, s, H-4), 8.28 (1H, s, N′-H), 7.90 (1H, d, J = 2.4 Hz, H-4′), 7.24 (1H, d, J = 8.4 Hz, H-6), 7.12 (1H, m, H-7′), 7.04 (1H, d, J = 8.4 Hz, H-7), 6.99 (1H, dd, J = 8.4, 2.4 Hz, H-6′), 3.33 (3H, s, OCH_3). HRMS (EI) $[M]^{+\bullet}$ ($C_{18}H_{12}F_3N_3O_4$): calcd 391.0780, found 391.0782.

Molecular Docking. Molecular docking was performed using CDOCKER, a CHARMm-based molecular dynamics docking algorithm on Discovery Studio 2.0 (Accelrys). The CDK2 structure cocrystallized with 5-bromo-indirubin was obtained from the PDB data bank (PDB code: 2BHE).[31] A protein clean process and a CHARMm-force field were sequentially applied. The area around 5-bromo-indirubin was chosen as the active site, with a radius set as 8 Å. After removing the ligand from the structure of the complex, a binding sphere in the three axis directions was constructed around the active site. All default parameters were used in the docking process. CHARMm-based molecular dynamics (1000 steps) were used to generate random ligand **3a** conformations, and the position of any ligand **3a** was optimized in the binding site using rigid body rotation followed by simulated annealing at 700 K. Final energy minimization was set as the full potential mode. The final binding conformation of **3a** was determined on the basis of energy. Docking study of ligand **2** was carried out as described above. The most stable binding mode among the top 10 of docking poses of each compound was presented in Figure 2. The other binding modes of compounds **2**, **3a** were not identified because of their similar docking poses, and the differences of calculated CDOCKER interaction energy were in the range of 4 kcal/mol.

Biological Methods. Enzyme Assay. CDK1/cyclin B, CDK2/cyclin E activities were assayed by using radiometric filter binding format.[39] CDK1/cyclin B was purchased from Millipore (Billerica, MA). In final reaction volume of 25 μL, CDK1/cyclin B was incubated in buffer (8 mM MOPS pH 7.0, 0.2 mM EDTA, 10 mM Mg acetate), with 0.1 mg/mL histone H1 and 45 μM [γ-^{33}P] ATP (500 cpm/pmol). The reaction was initiated by the addition of the MgATP mix. After incubation for 40 min at 30 °C, the reaction was stopped by the addition of 5 μL of 3% phosphoric acid solution. Ten μL aliquots of supernatant were spotted onto 2.5 cm ×3 cm pieces of Whatman P30 phosphocellulose paper, and 20 s later, the filters were washed three times for 5 min in 75 mM phosphoric acid and once in methanol prior to drying. The wet filters were counted in the presence of 1 mL of ACS (Amersham) scintillation fluid.

CDK2/cyclin E was purchased from Millipore (Billerica, MA). The kinase activity was tested in buffer (8 mM MOPS pH 7.0, 0.2 mM EDTA, 10 mM Mg acetate), with 0.1 mg/mL histone H1, in the presence of 120 μM [γ-^{33}P] ATP (500 cpm/pmol) in a final reaction volume of 25 μL. The reaction was initiated by the addition of the MgATP mix. After incubation for 40 min at 30 °C, the reaction was stopped by the addition of 5 μL of 3% phosphoric acid solution. Ten μL aliquots of supernatant were processed as described above.

Inhibition of kinase activity against a variety of recombinant kinases (c-Met, Met M1250T, Ron, VEGFR2, EGFR, TrkA, PI3Kγ, IKKβ, Insulin receptor, Aurora A) was determined by measuring the phosphorylation of substrate peptide or lipid in homogeneous time-resolved fluorescence (HTRF) assays.[40] The inhibition of tyrosine kinases, c-Met, Met M1250T, Ron, VEGF2, EGFR, TrkA, and insulin receptor was determined

by measuring the phosphorylation of poly-Glu-Tyr-biotin (pGT-biotin, Cisbio) peptide, HTRF KinEASE kit. Recombinant proteins containing kinase domain were purchased from Millipore (Billerica, MA). Into a black 384-well Costar plate was added 2 μL/well of serially diluted compound with kinase buffer (250 mM HEPES (pH 7.0), 0.5 mM orthovanadate, 0.05% BSA, 0.1% NaN_3). Next, 2 μL of TK peptide substrate and 1 μL of kinase (10 ng) were added to each well. After 15 min preincubation, the kinase reaction was initiated by the addition of 5 μL of ATP (2× the required final concentration) in reaction buffer, after which the plate was incubated at room temperature for 30 min. The reaction was stopped by the addition of 5 μL of TK-antibody-Eu(K) (Eu-labeled antiphosphotyrosine antibody, Cisbio) in HTRF detection buffer (50 mM HEPES (pH 7.0), 0.05% BSA, 0.1% NaN_3, and 100 mM EDTA) and 5 μL of streptavidin-XL-665 in HTRF detection buffer. After additional 1 h incubation at room temperature, the plate was read in an EnVision multilabel reader (Perkin-Elmer, Waltham, MA).

Recombinant proteins for IKKβ and Aurora A were purchased from Millipore (Billerica, MA). Assay was processed as described above, except for using the STK substrate-biotin-2 peptide (Aurora A), STK substrate-biotin-3 peptide (IKKβ).

The followings are ATP and supplement concentration for each enzyme: VEGFR2 (15 μM ATP, 5 mM $MgCl_2$, 1 mM $MnCl_2$, and 1 mM DTT), c-MET and MET M1250T (10 μM ATP, 5 mM $MgCl_2$, and 1 mM DTT), Ron (5 μM ATP, 5 mM $MgCl_2$, 1 mM $MnCl_2$, and 1 mM DTT), TrkA (1 μM ATP, 5 mM $MgCl_2$, and 1 mM DTT), insulin receptor (20 μM ATP, 5 mM $MgCl_2$, 1 mM $MnCl_2$, and 1 mM DTT), IKKβ (2 μM ATP, 2 mM $MnCl_2$, and 1 mM DTT), Aurora A (100 μM ATP, 5 mM $MnCl_2$, and 1 mM DTT), and EGFR (2 μM ATP, 5 mM $MgCl_2$, 1 mM $MnCl_2$, and 1 mM DTT).

Inhibition of PI3Kγ activity was measured by commercial kit from upstate (PI3-kinase (human) HTRF assay, catalogue no. 33-016). PI3K catalyzes the phosphorylation of phosphoinositol 4,5-biphosphate (PIP2) to phosphoinositol 3,4,5-triphosphate (PIP3). The PIP3 product formed by PI3K activity displaces biotin-PIP3 resulting in a loss of energy transfer and thus a decrease in signal. Kinase reaction was performed exactly as described in the manufacturer's instruction.

Cell Proliferation Assay. Cells (A549, HT1080, HCT116, K562, SNU638, KB, MCF-7) were counted, diluted to 5×10^4 cells/mL with fresh medium (MEME, DMEM, or RPMI containing 10% FBS), and added 190 μL of cell suspension to 96-well plates containing various concentrations of test compounds (10 μL in 10% aq DMSO).[41] Test plates were incubated for 3 days at 37 °C in CO_2 incubator. For zero day controls, cells were incubated for 30 min at 37 °C in CO_2 incubator. All treatments were performed in triplicate. After the incubation periods, cells were fixed with 50 μL of cold 50% TCA at 4 °C for 30 min, washed 5 times with tap water, and air-dried. The fixed cells were stained with 0.4% SRB solution in 1% aqueous acetic acid at room temperature for 1 h. Free SRB solution was then removed by rinsing 5 times with 1% acetic acid, and air-dried. The bound dye was dissolved with 200 μL of 10 mM Tris-base (pH 10.0), and absorbance was determined at 515 nm using an ELISA microplate reader. Finally, the absorbance values obtained with each of the treatment procedures were averaged, and the average values obtained with the zero day control were subtracted. These results were expressed as a percentage, relative to solvent treated control incubations, and IC_{50} values were calculated using nonlinear regression analysis (percent survival versus concentration).

Animal Tumor Model. The k-ras-transformed rat kidney epithelial cell line (RK3E-ras) were maintained in DMEM supplemented with 10% FCS, 100 units/mL penicillin, and 100 Ag/mL streptomycin. RK3E-ras cells were kindly provided by Dr. Eric Fearon (University of Michigan Medical School, Ann Arbor, MI) and have been described in the previous report.[36] Male SD rats (6 weeks of age) were used to examine the inhibition of tumor growth in vivo. RK3E-ras-Luc cells (5×10^6) were implanted subcutaneously into the flank of the rats on day 0, and rats were grouped randomly (5 mice/group) on day 5 as previously described.[36] A solution of **3a** in a mixture of PEG400, EtOH, and DW (30:33:37, 3 mg/mL, 5 mg/kg) were delivered intravenously in a nonanesthesia state every other day for a total of five times. The animals were sacrificed 48 h after the final administration, and rat weights and tumor volumes were measured. The tumor growth volumes were calculated as follows: $V = (ab^2)/2$, where, a is the longest diameter and b is the shortest diameter of the tumor.[36] All experiments were conducted under protocols approved by the Animal Care and Use Committee at Chosun University School of Dentistry (Gwangju, South Korea).

Bioluminescence Imaging Assay. For bioluminescence imaging, the rats received an ip injection of luciferin (Molecular Probes, Palo Alto, CA) with Rompun/ketamine (1:1) anesthesia. The rats were imaged using a LAS-1000 plus imaging System (Fuji film. Tokyo, Japan) to record the bioluminescent signal emitted from the tumor. The LAS-1000 system equipped with a CCD camera was used for acquisition of the emitted light, and Living Image software (Multi Gauge v3.0) was used for data analysis.

Histology, Immunohistochemistry, and TUNEL Assay. The excised solid tumors were fixed in 10% buffered formalin and embedded in paraffin. For optical microscopic examinations, 4 μm sectioned tissues were stained with H&E. Immunohistochemical staining was performed with the avidin−biotin complex method using anti-PCNA antibodies. The immune reactions were visualized with 3,3′-diaminobenzidine and counterstained with Mayer's hematoxylin. A TUNEL assay was performed using an ApopTag Plus peroxidase in situ apoptosis detection kit (Intergen, Purchase, NY) according to the manufacturer's instructions. Briefly, the slides were deparaffinized and treated with 20 μg/mL proteinase K at 37 °C for 15 min to enhance staining. After immersion in 3% hydrogen peroxide to block the endogenous peroxidase, the slides were incubated with a reaction buffer containing terminal deoxynucleotidyl transferase at 37 °C for 1 h. The slides were then incubated with a peroxidase-conjugated antidigoxigenin antibody for 30 min, and the reaction products were visualized with a 0.03% 3,3′-diaminobenzidine solution containing 2 mM hydrogen peroxide. The slides were counterstained with 0.5% methyl green. The PCNA and TUNEL-positive cells were counted and represented as the average of the five highest areas within a single ×200 field.[36]

Acknowledgment. This work was supported by a grant of the National R&D Program for Cancer Control, Ministry of Health & Welfare, Republic of Korea (0720430) and by a grant from the Institute of Medical System Engineering (iMSE) in the GIST, Korea. The work performed by S.-M. Kwon, S.-G. Ahn, and J.-H. Yoon was supported by the Korea Science and Engineering Foundation (KOSEF) grant funded by the Korea government (MOST) (no. R13-2008-010-01001-0).

Supporting Information Available: IC_{50} values of antiproliferative activity including mean ± SD, FACS analysis data of **3a**, analytical data of HPLC analysis of final compounds for purity, solubility data of compound **1**, **2**, **3a**. This material is available free of charge via the Internet at http://pubs.acs.org.

References

(1) Harper, J. W.; Adams, P. D. Cyclin-dependent kinases. *Chem. Rev.* **2001**, *101*, 2511–2526.
(2) Morgan, D. O. Principles of CDK regulation. *Nature* **1995**, *374*, 131–134.

(3) Dyson, N. The regulation of E2F by pRB-family proteins. *Genes Dev*. **1998**, *12*, 2245–2262.
(4) Weinberg, R. A. The retinoblastoma protein and cell cycle control. *Cell* **1995**, *81*, 323–330.
(5) Chen, Y. N. P.; Sharma, S. K.; Ramsey, T. M.; Jiang, L.; Martin, M. S.; Baker, K.; Adams, P. D.; Bair, K. W.; Kaelin, W. G., Jr. Selective killing of transformed cells by cyclin/cyclin-dependent kinase 2 antagonists. *Proc. Natl. Acad. Sci. U.S.A*. **1999**, *96*, 4325–4329.
(6) Shapiro, G. I.; Harper, J. W. Anticancer drug targets: cell cycle and checkpoint control. *J. Clin. Invest*. **1999**, *104*, 1645–1653.
(7) Van Den Heuvel, S.; Harlow, E. Distinct roles for cyclin-dependent kinases in cell cycle control. *Science* **1993**, *262*, 2050–2054.
(8) Loyer, P.; Trembley, J. H.; Katona, R.; Kidd, V. J.; Lahti, J. M. Role of CDK/cyclin complexes in transcription and RNA splicing. *Cell. Signalling* **2005**, *17*, 1033–1051.
(9) Zhao, J.; Kennedy, B. K.; Lawrence, B. D.; Barbie, D. A.; Gregory Matera, A.; Fletcher, J. A.; Harlow, E. NPAT links cyclin E-Cdk2 to the regulation of replication-dependent histone gene transcription. *Genes Dev*. **2000**, *14*, 2283–2297.
(10) Malumbres, M.; Barbacid, M. To cycle or not to cycle: a critical decision in cancer. *Nat. Rev. Cancer* **2001**, *1*, 222–231.
(11) Porter, P. L.; Malone, K. E.; Heagerty, P. J.; Alexander, G. M.; Gatti, L. A.; Firpo, E. J.; Daling, J. R.; Roberts, J. M. Expression of cell-cycle regulators p27 (Kip1) and cyclin E, alone and in combination, correlate with survival in young breast cancer patients. *Nat. Med*. **1997**, *3*, 222–225.
(12) Schraml, P.; Bucher, C.; Bissig, H.; Nocito, A.; Haas, P.; Wilber, K.; Seelig, S.; Kononen, J.; Mihatsch, M. J.; Dirnhofer, S.; Sauter, G. Cyclin E overexpression and amplification in human tumours. *J. Pathol*. **2003**, *200*, 375–382.
(13) Soria, J. C.; Se Jin, J.; Khuri, F. R.; Hassan, K.; Liu, D.; Waun, Ki, H.; Mao, L. Overexpression of cyclin B1 in early-stage non-small cell lung cancer and its clinical implication. *Cancer Res*. **2000**, *60*, 4000–4004.
(14) Takeno, S.; Noguchi, T.; Kikuchi, R.; Uchida, Y.; Yokoyama, S.; Muller, W. Prognostic value of cyclin B1 in patients with esophageal squamous cell carcinoma. *Cancer* **2002**, *94*, 2874–2881.
(15) Tetsu, O.; McCormick, F. Proliferation of cancer cells despite CDK2 inhibition. *Cancer Cell* **2003**, *3*, 233–245.
(16) Du, J.; Widlund, H. R.; Horstmann, M. A.; Ramaswamy, S.; Ross, K.; Huber, W. E.; Nishimura, E. K.; Golub, T. R.; Fisher, D. E. Critical role of CDK2 for melanoma growth linked to its melanocyte-specific transcriptional regulation by MITF. *Cancer Cell* **2004**, *6*, 565–576.
(17) Hanse, E. A.; Nelsen, C. J.; Goggin, M. M.; Anttila, C. K.; Mullany, L. K.; Berthet, C.; Kaldis, P.; Crary, G. S.; Kuriyama, R.; Albrecht, J. H. Cdk2 plays a critical role in hepatocyte cell cycle progression and survival in the setting of cyclin D1 expression in vivo. *Cell Cycle* **2009**, *8*, 2802–2809.
(18) Cai, D.; Latham, V. M., Jr.; Zhang, X.; Shapiro, G. I. Combined depletion of cell cycle and transcriptional cyclin-dependent kinase activities induces apoptosis in cancer cells. *Cancer Res*. **2006**, *66*, 9270–9280.
(19) Fischer, P. M.; Gianella-Borradori, A. Recent progress in the discovery and development of cyclin-dependent kinase inhibitors. *Expert Opin. Invest. Drugs* **2005**, *14*, 457–477.
(20) McClue, S. J.; Blake, D.; Clarke, R.; Cowan, A.; Cummings, L.; Fischer, P. M.; MacKenzie, M.; Melville, J.; Stewart, K.; Wang, S.; Zhelev, N.; Zheleva, D.; Lane, D. P. In vitro and in vivo antitumor properties of the cyclin dependent kinase inhibitor CYC202 (R-roscovitine). *In. J. Cancer* **2002**, *102*, 463–468.
(21) Misra, R. N.; Xiao, H. Y.; Kim, K. S.; Lu, S.; Han, W. C.; Barbosa, S. A.; Hunt, J. T.; Rawlins, D. B.; Shan, W.; Ahmed, S. Z.; Qian, L.; Chen, B. C.; Zhao, R.; Bednarz, M. S.; Kellar, K. A.; Mulheron, J. G.; Batorsky, R.; Roongta, U.; Kamath, A.; Marathe, P.; Ranadive, S. A.; Sack, J. S.; Tokarski, J. S.; Pavletich, N. P.; Lee, F. Y. F.; Webster, K. R.; Kimball, S. D. *N*-(Cycloalkylamino)-acyl-2-aminothiazole Inhibitors of Cyclin-Dependent Kinase 2. *N*-[5-[[[5-(1,1-Dimethylethyl)-2-oxazolyl]methyl]thio]-2-thiazolyl]-4-piperidinecarboxamide (BMS-387032), a Highly Efficacious and Selective Antitumor Agent. *J. Med. Chem*. **2004**, *47*, 1719–1728.
(22) Toogood, P. L.; Harvey, P. J.; Repine, J. T.; Sheehan, D. J.; VanderWel, S. N.; Zhou, H.; Keller, P. R.; McNamara, D. J.; Sherry, D.; Zhu, T.; Brodfuehrer, J.; Choi, C.; Barvian, M. R.; Fry, D. W. Discovery of a potent and selective inhibitor of cyclin-dependent kinase 4/6. *J. Med. Chem*. **2005**, *48*, 2388–2406.
(23) Moon, M. J.; Lee, S. K.; Lee, J. W.; Song, W. K.; Kim, S. W.; Kim, J. I.; Cho, C.; Choi, S. J.; Kim, Y. C. Synthesis and structure−activity relationships of novel indirubin derivatives as potent antiproliferative agents with CDK2 inhibitory activities. *Bioorg. Med. Chem*. **2006**, *14*, 237–246.
(24) Myrianthopoulos, V.; Magiatis, P.; Ferandin, Y.; Skaltsounis, A. L.; Meijer, L.; Mikros, E. An integrated computational approach to the phenomenon of potent and selective inhibition of aurora kinases B and C by a series of 7-substituted indirubins. *J. Med. Chem*. **2007**, *50*, 4027–4037.
(25) Vougogiannopoulou, K.; Ferandin, Y.; Bettayeb, K.; Myrianthopoulos, V.; Lozach, O.; Fan, Y.; Johnson, C. H.; Magiatis, P.; Skaltsounis, A. L.; Mikros, E.; Meijer, L. Soluble 3′,6-substituted indirubins with enhanced selectivity toward glycogen synthase kinase −3 alter circadian period. *J. Med. Chem*. **2008**, *51*, 6421–6431.
(26) Beauchard, A.; Laborie, H.; Rouillard, H.; Lozach, O.; Ferandin, Y.; Guevel, R. L.; Guguen-Guillouzo, C.; Meijer, L.; Besson, T.; Thiery, V. Synthesis and kinase inhibitory activity of novel substituted indigoids. *Bioorg. Med. Chem*. **2009**, *17*, 6257–6263.
(27) Lee, M. J.; Kim, M. Y.; Mo, J. S.; Ann, E. J.; Seo, M. S.; Hong, J. A.; Kim, Y. C.; Park, H. S. Indirubin-3′-monoxime, a derivative of a Chinese anti-leukemia medicine, inhibits Notch1 signaling. *Cancer Lett*. **2008**, *265*, 215–225.
(28) Yoon, J. H.; Kim, S. A.; Kwon, S. M.; Park, J. H.; Park, H. S.; Kim, Y. C.; Yoon, J. H.; Ahn, S. G. 5′-Nitro-indirubinoxime induces G1 cell cycle arrest and apoptosis in salivary gland adenocarcinoma cells through the inhibition of Notch-1 signaling. *Biochim. Biophys. Acta* **2010**, *1800*, 352–358.
(29) Park, E. J.; Choi, S. J.; Kim, Y. C.; Lee, S. H.; Park, S. W.; Lee, S. K. Novel small molecule activators of β-catenin-mediated signaling pathway: structure−activity relationships of indirubins. *Bioorg. Med. Chem. Lett*. **2009**, *19*, 2282–2284.
(30) Kim, S. H.; Kim, S. W.; Choi, S. J.; Kim, Y. C.; Kim, T. S. Enhancing effect of indirubin derivatives on 1,25-dihydroxyvitamin D_3- and all-*trans* retinoic acid-induced differentiation of HL-60 leukemia cells. *Bioorg. Med. Chem*. **2006**, *14*, 6752–6758.
(31) Jautelat, R.; Brumby, T.; Schafer, M.; Briem, H.; Eisenbrand, G.; Schwahn, S.; Kruger, M.; Lucking, U.; Prien, O.; Siemeister, G. From the insoluble dye indirubin towards highly active, soluble CDK2-inhibitors. *ChemBioChem* **2005**, *6*, 531–540.
(32) Helen, C. F.; Su; Tsou, K. C. Synthesis of bromo-substituted indoxyl esters for cytochemical demonstration of enzyme activity. *Cytochem. Demon. Enzyme Act*. **1960**, *82*, 1187–1189.
(33) Woodhead, A. J.; Berdini, V.; Boulstridge, J. A.; Carr, M. G.; Cross, D. M.; Davis, D. J.; Devine, L. A.; Early, T. R.; Feltell, R. E.; Lewis, E. J.; McMenamin, R. L.; Navarro, E. F.; O'Brien, M. A.; O'Reilly, M.; Reule, M.; Saxty, G.; Seavers, L. C. A.; Smith, D.-M.; Squires, M. S.; Trewartha, G.; Walker, M. T.; Woolford, A. J. A. Identification of *N*-(4-Piperidinyl)-4-(2,6-dichlorobenzoylamino)-1*H*-pyrazole-3-carboxamide (AT7519), a Novel Cyclin Dependent Kinase Inhibitor Using Fragment-Based X-Ray Crystallography and Structure Based Drug Design. *J. Med. Chem*. **2008**, *51*, 4986–4999.
(34) Beauchard, A.; Ferandin, Y.; Frere, S.; Lozach, O.; Blairvacq, M.; Meijer, L.; Thiery, V.; Besson, T. Synthesis of novel 5-substituted indirubins as protein kinases inhibitors. *Bioorg. Med. Chem*. **2006**, *14*, 6434–6443.
(35) Shtutman, M.; Zhurinsky, J.; Simcha, I.; Albanese, C.; D'Amico, M.; Pestell, R.; Ben-Ze'ev, A. The cyclin D1 gene is a target of the β-catenin/LEF-1 pathway. *Proc. Natl. Acad. Sci. U.S.A*. **1999**, *96*, 5522–5527.
(36) Kim, S.-A.; Kim, Y.-C.; Kim, S.-W.; Lee, S.-H.; Min, J.-J.; Ahn, S.-G.; Yoon, J.-H. Antitumor Activity of Novel Indirubin Derivatives in Rat Tumor Model. *Clin. Cancer Res*. **2007**, *13*, 253–259.
(37) Nam, S.; Buettner, R.; Turkson, J.; Kim, D.; Cheng, J. Q.; Muehlbeyer, S.; Hippe, F.; Vatter, S.; Merz, K. H.; Eisenbrand, G.; Jove, R. Indirubin derivatives inhibit Stat3 signaling and induce apoptosis in human cancer cells. *Proc. Nat. Acad. Sci. U.S.A*. **2005**, *102*, 5998–6003.
(38) Kim, S. A.; Kim, S. W.; Chang, S.; Yoon, J. H.; Ahn, S. G. 5′-Nitro-indirubinoxime induces G2/M cell cycle arrest and apoptosis in human KB oral carcinoma cells. *Cancer Lett*. **2009**, *274*, 72–77.
(39) Bain, J.; Mclauchlan, H.; Elliott, M.; Cohen, P. The specificities of protein kinase inhibitors: an update. *Biochem. J*. **2003**, *371*, 199–204.
(40) Pan, W.; Liu, H.; Xu, Y. J.; Chen, X.; Kim, K. H.; Milligan, D. L.; Columbus, J.; Hadari, Y. R.; Kussie, P.; Wong, W. C.; Labelle, M. Pyrimido-oxazepine as a versatile template for the development of inhibitors of specific kinases. *Bioorg. Med. Chem. Lett*. **2005**, *15*, 5474–5477.
(41) Skehan, P.; Storeng, R.; Scudiero, D.; Monks, A.; McMahon, J.; Vistica, D.; Warren, J. T.; Bokesch, H.; Kenney, S.; Boyd, M. R. New colorimetric cytotoxicity assay for anticancer drug screening. *J. Natl. Cancer Inst*. **1990**, *82*, 1107–1112.